Appl. Phys. A 84, 317–321 (2006)
DOI: 10.1007/s00339-006-3621-1

Applied Physics A
Materials Science & Processing

A.S. ZENG[1]
M.J. ZHENG[1,✉]
L. MA[2]
W.Z. SHEN[1]

Etching temperature dependence of optical properties of the electrochemically etched *n*-GaAs

[1] Laboratory of Condensed Matter Spectroscopy and Opto-Electronic Physics, Department of Physics, Shanghai Jiao Tong University, Shanghai 200240, P.R. China
[2] School of Chemistry and Chemical Technology, Shanghai Jiao Tong University, Shanghai 200240, P.R. China

Received: 15 August 2005/Accepted: 27 April 2006
Published online: 1 June 2006 • **© Springer-Verlag 2006**

ABSTRACT The GaAs granular films have been prepared by electrochemical anodic etching of *n*-GaAs in HCl electrolyte at different etching temperatures. The microstructure and optical properties of the films were investigated by micro-Raman spectrum, atomic force microscopy (AFM) and photoluminescence (PL) spectroscopy. Raman spectra reveal marked redshift and broadening, which could be explained by phonon confinement model. Results show the GaAs nanocrystalline films have formed during the anodic etching process under certain chemical conditions. Two "infrared" PL bands at ∼ 860 nm and ∼ 920 nm and a strongly enhanced visible PL band envelope around 550 nm were observed in the film prepared at etching temperature of 50 °C. The "green" PL band envelope is attributed to both quantum confinement in GaAs nanocrystals and PL of Ga_2O_3 and As_2O_3. The results reveal that the energy band structure of GaAs granular films is closely related to the etching temperatures.

PACS 81.07.Bc; 78.30.Fs; 78.55.Cr

1 Introduction

In recent years the localized dissolution of semiconductors has attracted a great deal of interests because of the discovery of the visible light emitting properties of porous silicon and its potential applications in light emitting devices such as optoelectronic switches and logic gates [1, 2]. Anodic oxidation, due to its good features such as low temperature, the simplicity and low processing costs, has been an effective way to fabricate porous structure semiconductors, such as SiC [3], InP [4–6], GaP [7–12], and GaAs [13–16].

GaAs is an important semiconductor with a direct band gap (1.424 eV) and a large exciton Bohr diameter (19 nm) [17]. A great deal of interest has been generated in both the etching of GaAs and formation of an oxide layer on its surface due to their unique optical properties and various applications particularly in electronic devices and in dry/wet solar cells [18]. M. Hao et al. [19] have formed porous GaAs using a two-step anodization process. The rate and product of GaAs oxidation depend on several factors: illumination, the pH of the electrolyte [18]. The rate of these oxides increase by illumination because the carriers involve in oxide of GaAs are the valence bond holes. Working in strongly alkaline solutions prevents the growth of oxide layers but causes lattice dissolution, while working in neutral and acidic electrolytes favors oxide growth. Lots of works have been done to research the photoluminescence (PL) property of porous GaAs [13–16, 19], and some very interesting PL properties have been observed. Porous GaAs produced in HF solution using *p*-type GaAs exhibits an "infrared" PL band and a "yellow" PL band [14]. And porous GaAs fabricated in HCl solution using *n*-type GaAs shows an "infrared" PL band and a "green" PL band [15]. Both the "yellow" PL band and the "green" PL band were explained by the quantum effect in nano-sized GaAs crystallites. However, there is no report about the relationship between the optical properties of electrochemical etched GaAs and etching temperature, and the origin of "green" PL band is still not completely understood.

In our work, the GaAs granular films have been prepared by electrochemical anodic etching of *n*-GaAs in HCl electrolyte at different etching temperatures. The microstructure and optical properties of anodized GaAs are discussed in detail by using micro-Raman and temperature dependence PL spectra. The broad and asymmetric Raman peaks are observed in the anodized GaAs, which could be explained by phonon confinement effect. It is found that the GaAs granular films prepared at etching temperature of 50 °C reveals strongly enhanced visible photoluminescence, which could be attributed to both the quantum confinement in GaAs nanocrystals and PL of Ga_2O_3 and As_2O_3.

2 Experimental

The wafers used in this study are *n*-type GaAs(100) wafers doped with 2×10^{18} cm^{-3} Te and the area of each wafer is 0.5×0.5 cm^2. Prior to each experiment, the samples were degreased with acetone and extensively rinsed with deionized water and then blown dry in N_2. The samples were then pasted to the center of circinal sheet with a copper by silver pastern. The exposed part of the circinal sheet was covered with insulating paint. An o-ring was pressed against the sample when the circinal sheet copper was screwed down in a teflon electrochemical cell as the anode. Accordingly graphite was used as the cathode, and the electrolyte was

✉ Fax: +86-021-54741040, E-mail: mjzheng@sjtu.edu.cn

Sample group	Etching solution	Etching potential (V)	Etching temperature (°C)	Etching time (min)
A	HCl (0.1 M)	7	30	10
B	HCl (0.1 M)	7	50	10
C	HCl (0.1 M)	7	70	10

TABLE 1 Sample data

hydrochloric acid. All solutions were prepared from analytical grade chemicals and deionized water. Then the electrochemical etching carried out in the 0.1 M HCl electrolyte for 10 min under the constant anodizing voltage of 7 V and electrolyte temperature of 30 °C, 50 °C and 70 °C, respectively. The sample data and preparation conditions are summarized in Table 1.

The biasing potentials as well as the polarization curve were recorded with an electrochemical analysis system (CHI618B). The AFM imaging was performed in air using a Digital Instruments Nanoscope IIIa in tapping mode. The Raman and PL spectra were recorded by a spectrometer with a liquid-nitrogen cooled charge coupled device detector, attached to a metallographic microscope. The Raman and PL excitation light sources were the 514.5 nm line of Ar^+ laser and the 325 nm line of ultraviolet laser, respectively.

3 Results and discussion

Figure 1 shows the Raman spectra at room temperature of the four samples (untreated GaAs, sample A, B and C). The Raman spectrum of untreated GaAs contains both the transverse optical (TO) band and longitudinal optical (LO) band. The peak positions of them are 272 and 295 cm^{-1}, respectively, which are coincident with the reported results [20]. For sample A and C, the two peak positions are almost consistent with those in untreated GaAs. While the intensities of TO bands and LO bands increase in comparison with untreated GaAs, which could be explained by the coupling of both the incident and the scattered fields with the low-order-structure resonance on the roughly etched surfaces [21]. However, for sample B, which was prepared by a potential of 7 V in 0.1 M HCl at 50 °C, the two Raman peak positions have been shifted down by nearly 12 cm^{-1} with respect to those in untreated GaAs. And the shapes of the LO and TO bands become markedly broader and asymmetric towards the lower energy tail in comparison with the usual sharp nature of untreated GaAs. Moreover, except for the two Raman peaks, some obviously new Raman peaks at 144, 167, 201, 417, and 475 cm^{-1} are observed.

The results [22] show that the smaller the size of crystalline particle is, the bigger the frequency shifts and the more asymmetric and the broader the peak becomes. So, from the characteristics of the Raman peaks (TO and LO) of sample B, it can be deduced that the nanocrystalline GaAs has formed in the etching layer of the sample B during anodic etching process. In order to estimate the size of GaAs nanocrystal particle, we fit the LO band of sample B with the "spatial correlation" model [23]. The Raman intensity, $I(\omega)$, at a frequency ω, can be obtained from the following equation:

$$I(\omega) \propto \int_0^1 \exp\left(\frac{-q^2L^2}{4}\right) \times \frac{d^3q}{[\omega-\omega(q)]^2+(\Gamma_0/2)^2}\,, \qquad (1)$$

where q is expressed in units of $2\pi/a$, a is the lattice constant of GaAs (0.564 nm), Γ_0 is the natural line width (full width at half maximum), L is the crystallite size, and $\omega(q)$ is the phonon dispersion curve. Based on an one-dimensional linear-chain model, the dispersion curve $\omega(q)$ of the LO phonon satisfies the following equation for GaAs [24]:

$$\omega^2(q) = A + \{A^2 - B[1-\cos(\pi q)]\}^{1/2}\,, \qquad (2)$$

which with $A = 4.14\times10^4\ cm^{-2}$ and $B = 7.11\times10^8\ cm^{-4}$ produces well the actual dispersion of the LO phonon in the etching layer of the sample B. The fitted curve of the LO band using (1) and (2) is shown in dashed line in Fig. 2, which is consistent with the experimental curve. And the corresponding fitted result of the size (L) of GaAs nanocrystal particle is about 6.1 nm. Moreover, an AFM image of the GaAs granular

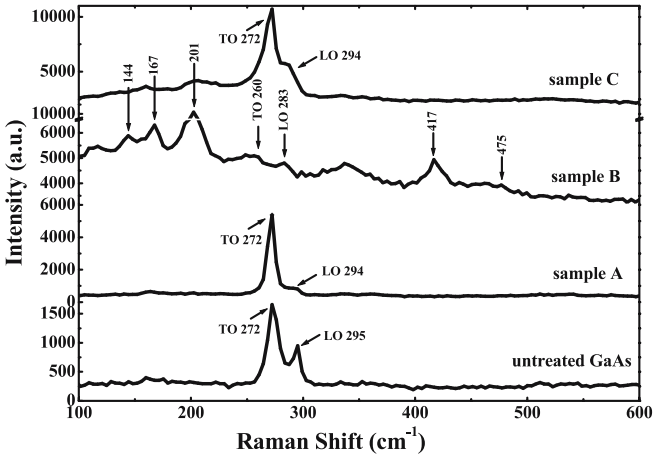

FIGURE 1 Raman spectra recorded at room temperature for different samples

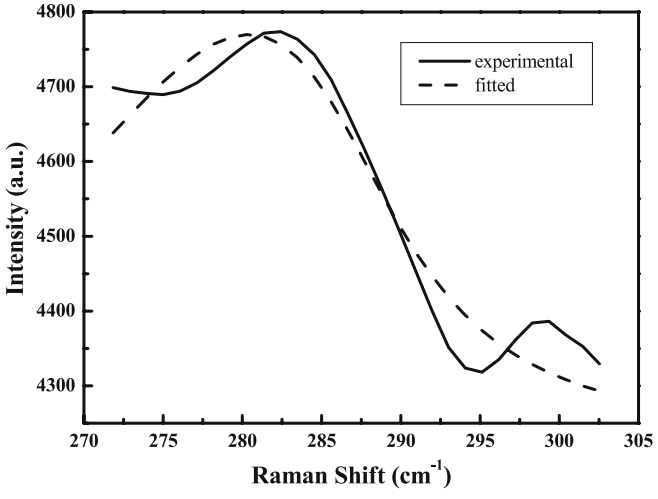

FIGURE 2 The LO band in the Raman spectrum of sample B prepared by a potential of 7 V in 0.1 M HCl at 50 °C and the theoretical fitted curve with the "spatial correlation" model

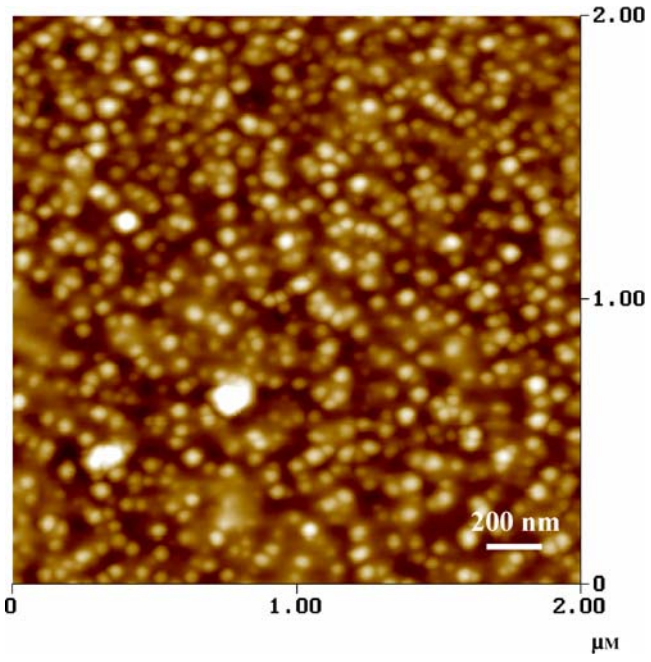

FIGURE 3 AFM image of the etched surface of sample B

films has been obtained to confirm the existence of the nano-sized GaAs particles in the etching layer, as shown in Fig. 3. Most of the particles on the sample surface have a diameter in the range of 15–40 nm which is larger than the predicted size of GaAs nanocrystal by the "spatial correlation" model. This may be caused by the agglomeration of several GaAs nanocrystal clusters or the mixing of GaAs nanocrystals and the oxides (Ga_2O_3 and As_2O_3 will be discussed later).

The redshift, broadening, and asymmetry of the Raman peaks can also be explained by the phonon confinement model [25]. Above results show that the size of the GaAs nanocrystals in sample B is smaller than the exciton Bohr diameter (19 nm). So the phonons suffer spatial confinement leading to decline in uncertainty in position. As a result, the uncertainty in its momentum goes up, relaxing the $q = 0$ selection rule. Now, the off Brillouin zone center phonons become active and appear towards the lower energy tail. The full spectrum is the result of superposition of all these off center phonons, which results in the redshift, broadening and asymmetry of the Raman peaks.

As we have mentioned, some obviously new Raman peaks at 144, 167, 201, 417, and 475 cm^{-1} were observed for the sample B. It's reported that the As_2O_3 Raman spectrum at room temperature is very strong with the most intense peaks at 85, 183, 268, 369, 414, 471, 560, and 781 cm^{-1}, while Ga_2O_3 has a relatively weaker spectrum with the most distinct peaks at 201, 418, and 769 cm^{-1} [16]. Comparing these parameters with the Raman spectrum of sample B, most of the new Raman peaks are attributed to As_2O_3 and peaks at 201, 417 cm^{-1} are associated with Ga_2O_3. This indicates the oxides (Ga_2O_3, As_2O_3) have been formed in the etching layer of sample B during electrochemical etching process. To further confirm the chemical composition in the etching layer of sample B, an energy dispersive X-ray (EDX) measurement is carried out. It is found that the etching layer consists of O, Ga and As. The atomic amount composition is 7.8% O, 53.6% Ga and 38.6% As. This result further supports our deduction about the formation of oxides (Ga_2O_3, As_2O_3) in the etching layer of sample B.

In order to make clear the process of oxidization during the anodic etching process, we used cyclic voltammetry (CV) in our discussion. The CV of the *n*-GaAs was carried out in 0.1 M HCl under electrolyte temperature of 50 °C and a rate of 50 mV/s. Figure 4 shows the polarization curve. The current density is less than 0.01 A/cm^2 when the anodic potential is smaller than 1.2 V, which could result from the formation of a blocking space charge layer (Schottky barrier) at the semiconductor/electrolyte interface by considering an *n*-type semiconductor/electrolyte junction under anodic bias [15]. After the turning point where the anodic potential is about 1.2 V, the current density has a distinct increase from 0.01 A/cm^2 to nearly 0.8 A/cm^2 until the anodic potential is about 4.7 V. This indicates the occurrence of the avalanche breakdown of the Schottky barrier and tunneling breakdown by considering the doping concentration at the turning point, and the surface of GaAs is dissolved by the following equation:

$$GaAs(s) + 6h^+ \rightarrow Ga^{3+}(aq) + As^{3+}(aq)\,. \qquad (3)$$

The Ga^{3+}, as well as the As^{3+}, is formed at the interface between electrolyte and solid phase, while the dispersed particles of Ga_2O_3, As_2O_3 and GaAs appear in the solution [13]. With the anodic potential raising from 4.7 V to 8 V, the current density exhibits a relatively steady range from 0.83 A/cm^2 to 0.78 A/cm^2, which shows the effective resistance of the etching layer becomes larger during this process. This could be attributed to the formation of oxides on the sample surface, which is consistent with the results of Raman spectra.

Figure 5 shows temperature dependence photoluminescence (PL) spectra of the samples (including untreated *n*-GaAs, sample A and C). The PL spectrum of sample B will be discussed in detail later. From Fig. 5, two obvious "in-

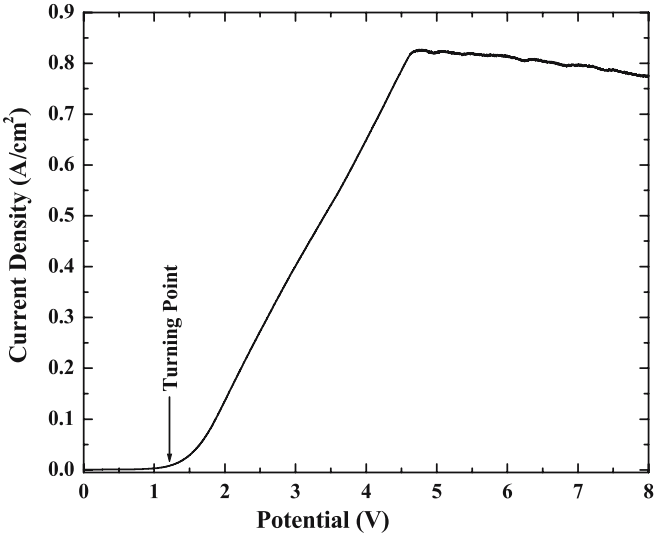

FIGURE 4 Polarization curves of *n*-GaAs (100) in 0.1 M HCl with a sweep rate of 50 mV/s

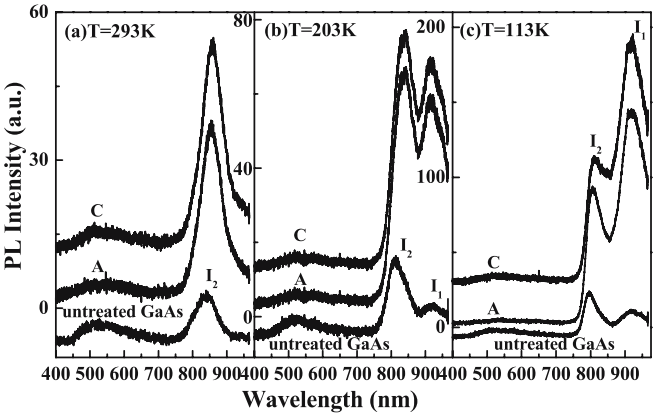

FIGURE 5 Temperature dependence PL spectra of untreated GaAs, sample A and C

frared" PL bands labeled as I_1 and I_2 can be seen when the PL temperatures are 203 K and 113 K but only one obvious PL band I_2 is observed at 293 K for the three samples. The PL band I_1 is seldom observed in the PL spectra of other reported work [13, 15, 16]. It has been reported [26] that the lifetime due to recombination involving impurity states was about 2.5 ns with the carrier concentration of $2 \times 10^{18}\,\mathrm{cm}^{-3}$, and the minimum radiative lifetimes for electrons equaled to 0.31 ns for *n*-GaAs. So the PL band I_1 could be associated with the continuum band – impurity level radiative recombination in our samples.

In order to assess the possible source of the PL band I_2, the corresponding PL temperature dependence of PL peak position and PL peak intensity of I_2 for the three samples is shown in Fig. 6. It can be found that, for each sample, the peak position of I_2 presents redshift and the corresponding peak intensity decreases with the rise of PL temperature. This is in accordance with the band gap narrowing and the peak intensity decreasing with increasing PL temperature in pure GaAs. So this PL band I_2 is attributed to the quasi-interband transition of Te-doped GaAs. When the PL temperature is 293 K, the peak positions of I_2 are 841, 854 and 859 nm in untreated *n*-GaAs, sample A and Sample C, respectively. This indicates that the energy band structure of the etching layer on the Te-doped GaAs is closely related to the etching temperature. Moreover, the intensities of the two "infrared" PL bands I_1 and I_2 of the electrochemical etched *n*-GaAs are markedly stronger than these of untreated *n*-GaAs, which could be attributed to the porosity [13, 14, 16] of the etching layer on *n*-GaAs surfaces.

Figure 7 shows the temperature dependence PL spectra of sample B that was prepared by a direct potential step to 7 V and holding this potential for 10 min with an etching temperature of 50 °C. It can be found that besides the two "infrared" PL bands, a markedly broad "green" band envelope around $450 \sim 650$ nm appears in each PL spectrum of sample B. But for untreated GaAs, sample A and C, the "green" PL band envelope is very weak and almost hard to be seen (see Fig. 5). The broad "green" PL band envelope in sample B can be fitted as two different PL bands labeled as I_3 and I_4 in Fig. 7 by Gaussian distribution model. It is found that the peak center of I_3 shifts from 550 nm to 590 nm with the increase of PL temperature, whereas the peak center of I_4 (from 475 nm to 515 nm) shows no correlation with the PL temperature.

For sample B, the size of GaAs nanocrystal has been calculated to be about 6.1 nm, which is smaller than the exciton Bohr diameter of GaAs (19 nm). According to the quantum confinement effect, the optical band gap of GaAs nanocrystal should be blue-shifted with respect to the bulk band gap. The band gap $E_{\max}$ of the GaAs nanocrystal can be estimated using the effective mass theory developed by Brus [27]:

$$E_{\max} = \frac{\hbar^2\pi^2}{2d^2}\left(\frac{1}{m_{\mathrm{e}}^*} + \frac{1}{m_{\mathrm{h}}^*}\right) - \frac{1.8e^2}{\varepsilon d} + E_{\mathrm{g}}\,, \tag{4}$$

where E_{g} is the band gap of GaAs with value 1.424 eV, d is the size of GaAs nanocrystal (6.1 nm), m_{e}^* and m_{h}^* are the effective masses of electron and hole with values 0.063 and 0.53 [16], respectively, ε is the high frequency dielectric constant that equals to 10.9, and $e^2 = 1.44$ eV nm. From the (4) and data above, we can estimate $E_{\max}$ to be 2.129 eV (583 nm), which is corresponding to the room temperature (293 K) PL peak position of I_3. So it can be deduced that the PL band I_3 results from the quantum confinement effect in GaAs nanocrystals.

Above Raman spectrum and EDX results have shown that an etching layer containing As_2O_3 and Ga_2O_3 has formed on

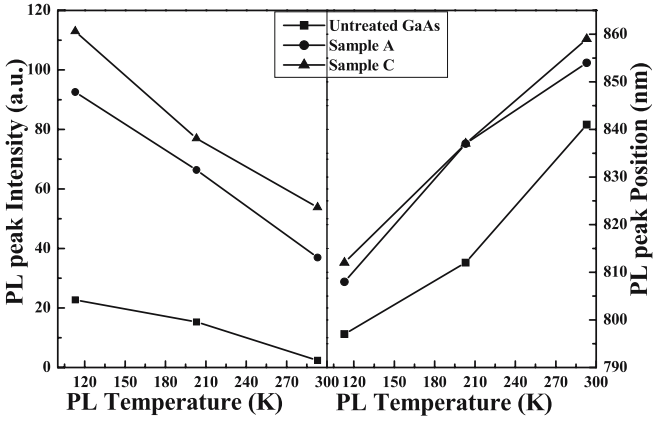

FIGURE 6 The PL temperature dependence of PL peak position and PL peak intensity of I_2 for untreated GaAs, sample A, and sample C

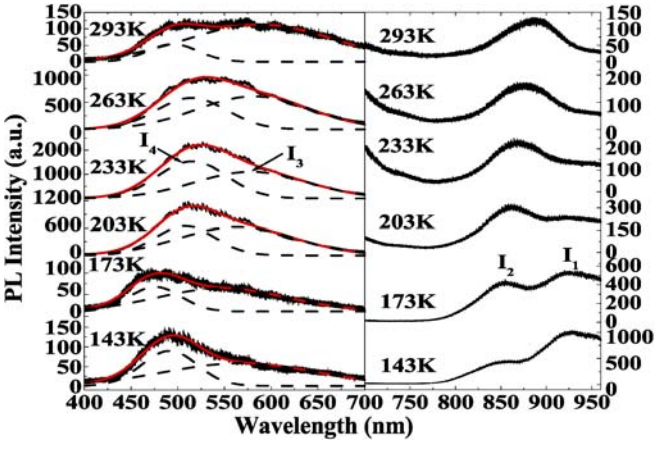

FIGURE 7 Temperature dependence PL spectra of sample B prepared by a potential of 7 V in 0.1 M HCl at 50 °C. The *dotted curves* are the corresponding fitted curves of the "green" PL band envelope

the surface of sample B during the anodic etching process. The PL peak of 540 nm and the PL peak of 475 nm have been observed for As_2O_3 [28] and Ga_2O_3 [29], respectively. So the I_4 PL band could be attributed to the photoluminescence of Ga_2O_3 and As_2O_3.

Above results show the "green" band envelopes in PL spectrum for the sample B could result from both the quantum confinement effect in GaAs nanocrystals and the photoluminescence of Ga_2O_3 and As_2O_3. While it is noticed that obviously new Raman peaks and the broad "green" band envelope have not been observed for anodic etched GaAs under higher etching temperatures (i.e., Raman spectrum of the sample C in Fig. 1 and PL spectra of the sample C in Fig. 5), which could be associated with either the brushing off of the oxides layer due to drastic reaction or the electropolishing on the sample surface during the etching process. These indicate that the microstructure changes of anodic etched GaAs under different etching temperatures result in the differences of their optical properties.

4 Conclusion

We have explored the microstructure and optical properties of the anodic etching layers of *n*-GaAs prepared at different etching temperatures. The Raman study reveals that the formation of GaAs nanocrystals and the oxides (Ga_2O_3, As_2O_3) on the etching layer is associated with the etching temperature, which is further confirmed by the AFM image and EDX analyses. The intensity of the two "infrared" PL bands I_1 and I_2 of the electrochemical etched *n*-GaAs is markedly stronger than that of untreated *n*-GaAs, while both the "infrared" PL bands do not reveal the systematic correlation with the etching temperatures. What is more interesting, for the sample prepared at etching temperature of 50 °C the broad "green" band envelope is stronger than any other samples, which is attributed to two factors: quantum confinement effect in GaAs nanocrystals and the photoluminescence of Ga_2O_3 and As_2O_3.

ACKNOWLEDGEMENTS This work was supported by the Natural Science Foundation of China under contract No.10125416 and No. 50572064, Shanghai Major Project of 03DJ14003, Shanghai Nanotechnology Fundamental Research Project of 0352nm013, and Shanghai Major Project of 03dz14014.

REFERENCES

1 A.G. Cullis, L.T. Canham, P.D.G. Calcott, J. Appl. Phys. **82**, 909 (1997)
2 P.M. Fauchet, IEEE J. Sel. Top. Quantum Electron. **4**, 1020 (1998)
3 J.S. Shor, I. Grimberg, B.Z. Weiss, A.D. Kurtz, Appl. Phys. Lett. **62**, 2836 (1993)
4 T. Takizawa, S. Arai, M. Nakahara, Jpn. J. Appl. Phys. 1 **33**, 2643 (1994)
5 N.G. Ferreira, D. Soltz, F. Decker, L. Cescato, J. Electrochem. Soc. **142**, 1348 (1995)
6 E. Kumino, M. Amiotto, T. Takizawa, S. Arai, Jpn. J. Appl. Phys. 1 **34**, 177 (1995)
7 A.I. Belogrokhov, V.A. Karavanskii, A.N. Obraztsov, V.Y. Timoshenko, JETP Lett. **60**, 275 (1994)
8 B.H. Erne, D. Vanmeakelbergh, J.J. Kelly, Adv. Mater. **7**, 739 (1995)
9 A. Aredda, A. Serpi, V.A. Karravanskii, I.M. Tiginyanu, V.M. Ichizli, Appl. Phys. Lett. **67**, 3316 (1995)
10 I.M. Tiginyanu, V.V. Ursaki, V.A. Karavanskii, V.N. Sokolov, Y.S. Raptis, E. Anastassakis, Solid State Commun. **97**, 675 (1996)
11 B.H. Erne, D. Vanmaekelbergh, J.J. Kelly, J. Electrochem. Soc. **143**, 305 (1996)
12 A. Meyerink, A.A. Bol, J.J. Kelly, Appl. Phys. Lett. **69**, 2801 (1996)
13 J. Sabataityte, I. Simkiene, R.A. Bendorius, K. Grigoras, V. Jasutis, V. Pacebutas, H. Tvardauskas, K. Naudzius, Mater. Sci. Eng. C **19**, 155 (2002)
14 L. Beji, L. Sfaxi, B. Ismail, S. Zghal, F. Hassen, H. Maaref, Microelectron. J. **34**, 969 (2003)
15 P. Schmuki, D.J. Lockwood, H.J. Labbe, J.W. Fraser, Appl. Phys. Lett. **69**, 1620 (1996)
16 D.J. Lockwood, P. Schmuki, H.J. Labbe, J.W. Fraser, Physica E **4**, 102 (1999)
17 J. Nayak, R. Mythili, M. Vijayalakshmi, S.N. Sahu, Physica E **24**, 227 (2004)
18 S.Y. Alqaradawi, A.S. Aljaber, M.M. Khader, Thin Solid Films **444**, 282 (2003)
19 M. Hao, H. Uchida, C. Shao, T. Soga, T. Jimbo, M. Umeno, J. Cryst. Growth **179**, 661 (1997)
20 K.K. Tiong, P.M. Amirtharaj, F.H. Pollak, D.E. Aspens, Appl. Phys. Lett. **44**, 122 (1984)
21 D.V. Murphy, S.R.J. Brueck, Opt. Lett. **8**, 494 (1983)
22 B.B. Li, D.P. Yu, S.L. Zhang, Phys. Rev. B. **59**, 1645 (1999)
23 P. Parayanthal, F.H. Pollak, Phys. Rev. Lett. **52**, 1822 (1984)
24 C. Kittel, *Introduction to Solid State Physics* (Wiley, New York, 1967), 3rd edn., Chapt. 5
25 H. Richter, Z.P. Wang, L. Ley, Solid State Commun. **39**, 625 (1981)
26 W.P. Dumke, Phys. Rev. **132**, 1998 (1963)
27 L.E. Brus, J. Chem. Phys. **80**, 4403 (1984)
28 J.I. Zlnk, B.P. Chandra, J. Phys. Chem. **86**, 5 (1982)
29 P. Guha, S. Chakrabarti, S. Chaudhuri, Physica E **23**, 81 (2004)